Nuclear Physics A382 (1982) 1–30

A GRAPHICAL PROCEDURE TO EVALUATE THE MANY-BODY SHELL-MODEL EQUATIONS

R. J. LIOTTA

Research Institute of Physics, S-10405 Stockholm 50, Sweden

and

C. POMAR

Departamento de Fisica, CNEA, Av. del Libertador 8250, 1429 Buenos Aires, Argentina

Received 9 December 1981

Abstract: The many-body shell-model equations are solved within the framework of a multistep shell-model method (MSM). It is found that there are many different ways to proceed through such a method. A graphical procedure to evaluate all the corresponding MSM equations is presented. Within this procedure one can easily visualize all those possibilities and quickly choose the most convenient one. This graphical procedure is applied to calculate ground-state energies and wave functions in many-nucleon systems and good agreement with experimental data is obtained.

1. Introduction

A recurrent theme in nuclear spectroscopy has recently been the use of correlated bases to describe many-body nuclear systems [1–12]. In spherical nuclei, these correlated bases consist of particle-particle (normal pairing vibration) and particle-hole (surface vibration) vector coupled states. In addition, single-particle states are kept as basis elements when necessary (i.e. to analyse nuclei with odd numbers of nucleons). Within such correlated bases one can span the shell-model space if no truncation is made. In this case, however, the dimensions of the correlated bases are much larger than the shell-model dimensions and the corresponding calculations become both prohibitive and not very meaningful. The reason why the correlated bases are generally overdimensioned (or "overcomplete" as overdimensioned bases are usually called) is that within these bases one may count twice the same state and also one may violate the Pauli principle. As a result, the elements of a correlated basis are not orthogonal to each other [occasionally, as in two-proton two-neutron excitation, the correlated basis is orthogonal [12]]. Therefore, to obtain the shell-model states one must first evaluate the metric (or overlap) matrix. One can then apply any of the available procedures to describe a vector using a non-orthogonal basis [4, 9, 13].

The fact that methods which use correlated bases allow us to obtain the shell-model

states is important, because within these methods one can carry out drastic truncations of the basis. Thus, although the full application of these methods is not meaningful, one is certain that vectors which are contained in small correlated subspaces are also shell-model vectors.

Even so, not many applications of such methods have up till now been performed to nuclei with more than four particles outside double-magic cores. This is partly due to the complexities associated with the formalism and the related difficulties of evaluating both the dynamical and the metric matrices. The formalism was eased by Ring and Schuck [5]) who realized that for three and four-particle systems the bare two-particle interaction could advantageously be replaced by the corresponding two-particle energies and wave functions. It was later realized that, in general, the equations corresponding to a many-body system in a correlated basis could be greatly simplified by replacing the bare interaction matrix elements by the correlated energies and wave functions of the subsystems that compose the basis [10, 14]). Moreover, the metric matrix could also be written in terms of quantities related to those subsystems. An additional advantage was that all these quantities could be calculated in previous steps of the case being considered (thus the name: multistep shell-model method). But such a replacement is not a trivial task. Not only skilful algebraical manipulations are required but also there might be many different ways to write the final equations in terms of the subsystem quantities. If one wishes to have the most convenient of all those possible equations, one must evaluate all of them, which may make the whole procedure a very tedious and difficult undertaking. To overcome these problems it was recently proposed to use a graphical method to evaluate the dynamical and metric equations [14]). We present here this graphical method in detail and apply it to the calculation of ground-state energies of nuclei with many nucleons outside closed shell cores. The formalism is given in sect. 2; in sect. 3 are the applications and our conclusions are given in sect. 4.

2. Multistep shell-model method – graphical procedure

As the shell-model is usually understood, one calculates a many-body system in two steps. First one takes the single-particle states given by a simple one-body interaction with single-particle energies as parameters fitted to experimental values. In the second step, one proceeds to the calculation of the energies and wave functions of the final system in the basis provided by the single-particle states calculated in the first step [15]).

In a way, the multistep shell-model method [10]) (MSM) is a generalization of that procedure. As in usual shell-model calculations, one first chooses a single-particle representation which defines the shell-model space. Then one proceeds to calculate the two-particle system. In this step, one assumes that the two-body interaction is well known or, alternatively, the interaction matrix elements are taken from experiment

[refs. [16-18])]. With the two-particle energies and wave functions thus calculated, one proceeds to the next step. Now one calculates the three-nucleon system in a basis which consists of the one- and two-particle vector-coupled states previously evaluated [refs. [2-5, 9])]. In the next step one can calculate the four-particle system in terms of the one- and three-particle states or in terms of the two-particle states – or both. In the same fashion, one proceeds forward with an increasing number of particles [refs. [10, 14])]. Of course, one does not need to calculate nucleus after nucleus up to the final step. For instance, the four-particle nucleus can be calculated directly from the two-particle states without going through the calculation of the three-particle system. Actually, this is the way that all four-particle calculations within correlated bases have so far been done [2-5, 10, 12]).

This MSM procedure presents the advantage that in a given step one can check the theoretical results against the corresponding experimental data. Moreover, since the energies calculated in a given step are used in a later step, these energies can be "renormalized" to the experimental values. As pointed out above, this procedure is followed in usual shell-model calculations with the single-particle states.

As shown in this section, the bare two-particle interaction can, within the MSM, be replaced by quantities related to the subsystems used to generate the MSM basis. This property greatly simplifies the formalism, since all the recoupling coefficients contained in the equations of a given step are not passed to later steps. One can say that the subsystems that form the MSM basis are like building blocks that one has painstakingly built in a given step to be used as a whole in a later step.

A drawback of the MSM basis is that it may contain elements that are both redundant and, maybe, violate the Pauli principle. As a result, the MSM basis is not an orthogonal basis. In fact, this drawback is shared by most methods and models that use correlated bases. As an exception one may mention the nuclear field theory [8]), although in this theory the metric of the space also appears [to properly evaluate the normalization of the NFT wave functions [19])] and its evaluation may not be easy [20]). In order to write a vector within an overcomplete basis, one must calculate the metric matrix, i.e. the overlap matrix among the basis elements [4, 9]). However, as shown in sect. 3, not always is it necessary to pass through the metric matrix in order to calculate some properties within the framework of the MSM.

The metric matrix can also be written in terms of quantities related to the subsystem used to form the MSM basis. But, as mentioned in the introduction, this procedure may not be an easy task, because rather complicated algebraic manipulations are required both for the dynamical and the metric equations. Moreover, there might be many different ways to write down the MSM equations and it might not be easy to find the most convenient (from a calculation viewpoint) of those possibilities. To overcome these difficulties, we present in this section a graphical procedure to evaluate the dynamical matrix, the metric matrix, and the MSM matrix elements of transition operators.

2.1. THE MSM BASIS

Let s be the number of particles of a given system σ. We assume σ to be divided into two subsystems μ and ν, with particle numbers m and n, respectively, such that $s = m+n$. The MSM set of basis vectors is given by

$$\{|\alpha_m\alpha_n;\alpha_s\rangle\} = \{(P^+(\alpha_m)P^+(\alpha_n))_{\alpha_s}|0\rangle\}, \tag{1}$$

where α_m, α_n and α_s label states of the systems μ, ν and σ, respectively. Throughout this paper we will use Greek letters to label states of a given system. The number of particles of the system will appear as an index, as in eq. (1). An exception will be the single-particle states which will be labelled with Latin letters, as usual. In all cases we use the same symbols to label states as well as the corresponding angular momenta, as seen in eq. (1). The core wave function is $|0\rangle$ while P^+ denotes creation operators. Again here we adopt the usual notation c^+ for the one-particle creation operator. Therefore, in our formalism a σ-state is given by

$$|\alpha_s\rangle = P^+(\alpha_s)|0\rangle, \tag{2.1}$$

$$P^+(\alpha_s) = (1+\delta_{nm})^{-1}\sum_{\alpha_m\alpha_n} Y(\alpha_m\alpha_n;\alpha_s)(P^+(\alpha_m)P^+(\alpha_n))_{\alpha_s}, \tag{2.2}$$

where

$$Y(\alpha_m\alpha_n;\alpha_s) = (1+\delta_{\alpha_m\alpha_n})X(\alpha_m\alpha_n;\alpha_s). \tag{2.3}$$

The factor $(1+\delta_{nm})^{-1}$ in eq. (2.2) takes care of the double counting in the summation for the case $m = n$. The surplus factor $\frac{1}{2}$ for $\alpha_m = \alpha_n$ is cancelled by the δ-function in (2.3). From eq. (2) one obtains

$$\delta_{\alpha_s\beta_s} = \sum_{\alpha_m(\leqslant)\alpha_n} X(\alpha_m\alpha_n;\alpha_s)X(\beta_s)(P^+(\alpha_m)P^+(\alpha_n))_{\alpha_s}|0\rangle, \tag{3}$$

where the symbols in parentheses in the summation indicate that the ordering is only valid for $n = m$. Eq. (3) shows that

$$X(\alpha_m\alpha_n;\beta_s) = \langle\beta_s|(P^+(\alpha_m)P^+(\alpha_n))_{\beta_s}|0\rangle^* \tag{4}$$

only if the basis (1) is orthonormal as, e.g., in the two-particle ($m = n = 1$) case. Although X is not well defined within an overcomplete basis [10]), the quantity

$$F(\alpha_m\alpha_n;\beta_s) = \langle\beta_s|(P^+(\alpha_m)P^+(\alpha_n))_{\beta_s}|\rangle \tag{5}$$

does not depend upon the basis (1). It simply represents the projection of the physical vector $|\beta_s\rangle$ onto the basis vector (1). Actually, the function F is closely related to the form factor of m- (or n-) particle transfer reactions [9, 10]).

We have chosen in eq. (2) a definite partition of the system σ in two subsystems. But one can have situations where a more general basis would be required. For instance, one may need (or like) to describe the four-particle system in terms of the

two possible partitions previously mentioned (i.e. $m = 1, n = 3$ and $m = 2, n = 2$) simultaneously. This example may sound as having a mere academic value. Yet, that is not the case for the two-particle one-hole excitations, where a simultaneous treatment of surface vibrations coupled to particles and pairing vibrations coupled to holes proved to be very fruitful in the lead region [21]). Other systems which may be conveniently written in terms of several partitions simultaneously are those where neutron and proton excitations have to be treated on the same footing. Although we do not treat such cases explicitly in this paper, the generalization of the procedure presented here to those situations is rather straightforward.

One may also describe a system in terms of three or more partitions. In fact, this is the way in which all microscopic methods and models have so far proceeded. For instance, in both the NFT [11]) and the IBA [7]) the calculation of a many-particle system is carried out within a many-boson basis.

We have written eqs. (1) and (2) coupled to good angular momenta. In the following, however, we will derive all equations in a decoupled basis. At the end we will use a graphical method to obtain the angular momentum coupling coefficients. In this way we will leave the possibility open for choosing expressions which would be formally simple both in the dynamical and kinematical parts.

2.2. DYNAMICAL MATRIX

The dynamical equations which control the behaviour of the system σ can be obtained using the Tamm-Dankoff approximation (TDA) as usual. That is, one writes the commutation $[H, P^+(\alpha_m)P^+(\alpha_n)]$ in normal form and keeps only linear terms in P^+P^+ (or its single-particle equivalent). However for our procedure it is more convenient to define the quantity

$$A(\alpha_m\alpha_n; \alpha_s) = \langle\alpha_s|[[H, P^+(\alpha_m)], P^+(\alpha_n)]_\pm|0\rangle. \tag{6}$$

The plus sign in the outside square brackets applies when both m and n are odd. Otherwise the square brackets indicate a commutation operation, as usual.

The hamiltonian H is given by

$$H = H_0 + V,$$

and H_0 is the one-body hamiltonian which provides the shell-model representation. Since $[H_0, P^+(\alpha_m)]$ is proportional to the product of m single-particle creation operators, one can as well write

$$A(\alpha_m\alpha_n; \alpha_s) = \langle\alpha_s|[[V, P^+(\alpha_m)], P^+(\alpha_n)]_\pm|0\rangle. \tag{7}$$

After some simple algebra eq. (6) gives

$$A(\alpha_m\alpha_n; \alpha_s) = (W_{\alpha_s} - W_{\alpha_m} - W_{\alpha_n})\, F(\alpha_m\alpha_n; \alpha_s), \tag{8}$$

where W is energy referred to the core but, as an exception, in this paper we will denote by $\varepsilon(\omega)$ the one- (two-) particle energy.

The most simple case that one can have in eq. (7) is $s = 2$ ($m = n = 1$). One easily finds

$$\Lambda(ij;\alpha_2) = \tfrac{1}{2}\sum_{kl}\langle kl|V|ij\rangle\langle\alpha_2|c_k^+ c_l^+|0\rangle, \tag{9}$$

which is the coupling constant of the nuclear field theory for the TDA pairing boson [22]. We will use the name "coupling constant" even for Λ in the general case of eq. (6).

To calculate this coupling constant one can write the operators P^+ in terms of their components [as in eq. (2)]. One can then write the resulting expression into normal form [23]. Since we assume the ground state $|0\rangle$ to be a shell-model (TDA) vacuum, only linear terms are kept. After this tedious calculation has been done, one finds that the two-body interaction appears in combinations that allow eq. (7) to be written in terms of the energies and wave functions of the μ- and ν-systems.

Instead of following this procedure, with all the difficulties mentioned in the previous subsection, we introduce a graphical method to evaluate Λ. We then represent a single-particle state by a straight line while all other states are represented by double lines. The labelling of the lines makes it clear to which system corresponds each line, as shown in fig. 1. To evaluate the coupling constant (7) one has first to write the operators P^+ in terms of their single-particle components. In fig. 2 we show the graphical representation of this decomposition for the cases $s = 2$ ($m = n = 1$) and $s = 4$ ($m = n = 2$) [notation as in eq. (2)]. In fig. 3 we present the graphical representation of eq. (2) for the case $s = 6$ ($m = 2$, $n = 4$). Here we have made the further assumption that the state α_4 is written in terms of two-particle states. Therefore the graphs in figs. 2 and 3 represent

(i) $|\alpha_2\rangle = \tfrac{1}{2}\sum_{ij} Y(ij;\alpha_2)c_i^+ c_j^+|0\rangle$ (fig. 2a);

(ii) $|\alpha_4\rangle = \tfrac{1}{8}\sum_{\alpha_2\beta_2}\sum_{ijkl} Y(\alpha_2\beta_2;\alpha_4)Y(ij;\alpha_2)Y(kl;\beta_2)c_i^+ c_j^+ c_k^+ c_l^+|0\rangle$ (fig. 2b);

(iii) $|\alpha_6\rangle = \tfrac{1}{16}\sum_{\alpha_4\alpha_2'}\sum_{\alpha_2\beta_2}\sum_{ijkl'l'} Y(\alpha_4\alpha_2';\alpha_6)$

$\times\, Y(\alpha_2\beta_2;\alpha_4)Y(ij;\alpha_2)Y(kl;\beta_2)Y(k'l';\alpha_2')c_i^+ c_j^+ c_k^+ c_l^+ c_{k'}^+ c_{l'}^+|0\rangle$. (fig. 3).

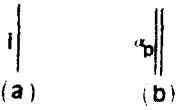

Fig. 1. (a) Graphical representation of the single-particle state $|i\rangle = c_i^+|0\rangle$. (b) Graphical representation of the state $|\alpha_\rho\rangle = P^+(\alpha_\rho)|0\rangle$. The number of particles corresponding to this state is $\rho = 1$.

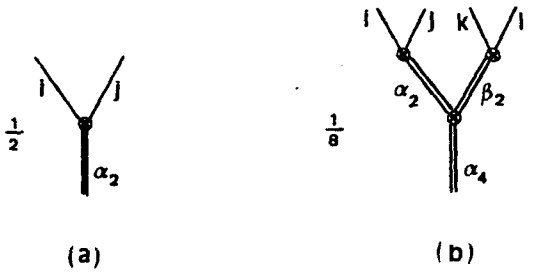

Fig. 2. Graphical representation of the decomposition of $P^{+}(\alpha_s)$ into its single-particle components [as in eq. (2)] for the cases (a) $s = 2$ ($m = n = 1$) and (b) $s = 4$ ($m = n = 2$). The crossed circles represent the amplitudes Y. The factors $\frac{1}{2}$ and $\frac{1}{8}$ in (a) and (b), respectively, are given by the δ-function in eq. (2.2).

It is important to remark that the graphs must be read from left to right. Thus the vertex in graph 2a represents $Y(ij;\alpha_2)$ and *not* $Y(ji;\alpha_2)$. In any other case one proceeds as in figs. 2 and 3.

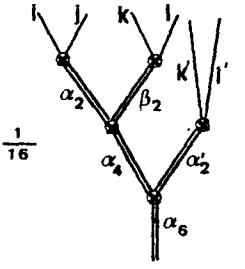

Fig. 3. As fig. 2 for the case $s = 6$ ($m = 4$, $n = 2$). In this case the crossed circle vertex that opens the line α_6 is not accompanied by the factor $\frac{1}{2}$ that goes with all the other vertices in this and the previous figure.

Since a double line will generally describe a many-particle state, we use in the following the name "block" to denote a double line and its decomposition into the corresponding components. Thus, fig. 3 is a six-particle block†.

To evaluate Λ graphically, one first decomposes the blocks α_m and α_n. Each contribution to Λ is obtained by joining two single-particle lines *belonging to different blocks* through a dashed line. This dashed line represents the interaction. Due to the double commutator in eq. (7), the quantity Λ does not contain contributions where single-particle lines belonging to the same block are joined. These contributions are already counted by the zero order contribution $\Lambda = 0$. With "zero order" we only mean that it would correspond to setting $V = 0$ in eq. (7). But, of course, our treatment is exact in the sense that we are exactly solving the shell-model equations.

† Note that when we refer to "graph" or "figure" or "block" we understand not only the graph itself but also the factors in front. Thus graph 3 also includes the factor $\frac{1}{16}$.

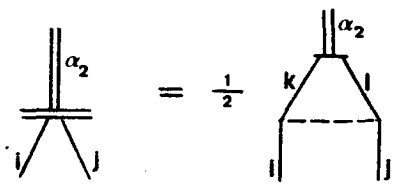

Fig. 4. Graphical representation of the pairing coupling constant [eq. (9)]. The double bar vertex represents Λ; the dashed line represents the interaction, and the one-bar vertex represents the overlap $F(kl;\alpha_2) = \langle\alpha_2|c_k^+ c_l^+|0\rangle$.

So far we have only given a recipe to account for "contractions", in the language of Wick's theorem [23]). Thus, lines of the same block must not be joined through a dashed line because that would imply that the single-particle destruction operators in V are contracted with components of $P^+(\alpha_m)$ (or $P^+(\alpha_n)$) in eq. (7). Then $[V, P^+(\alpha_m)]$ would be a product of creation operators and Λ would be zero.

After two lines have been joined, as described above, the diagram is completed, as shown in fig. 4, for the two-particle (pairing) coupling constant [eq. (9)]. In this simple case there is no doubt about how the single-particle lines have to be continued after the dashed line has been drawn, since only the possibility shown in fig. 4 exists. Moreover, the one-bar vertex is here simply related to the crossed circle vertex of fig. 2a. In fact, the only difference between them is a complex conjugate operation [see eq. (4)]. Graphically, this operation corresponds to reversing the vertices shown so far. Thus, in fig. 5 we give the graphical representation of the quantities $Y^*(\alpha_m\alpha_n;\alpha_s)$ and $\langle\alpha_d|P^+(\alpha_a)P^+(\alpha_b)\ldots P^+(\alpha_c)|0\rangle^*$. In general, the simple relation (4) between the one-bar and the crossed-circle vertices does not hold.

In fig. 6 we present the graphical representation of the three-particle coupling constant. Fig. 6b gives already a possible way to write Λ, i.e.

$$\Lambda(i\alpha_2;\alpha_3) = \tfrac{1}{2}\sum_{kljj'} X(jj';\alpha_2)\langle kl|V|ij\rangle\langle\alpha_3|c_k^+ c_l^+ c_{j'}^+|0\rangle. \tag{10}$$

This expression is the one that one would obtain within the usual shell-model formalism. But since, in general

$$\sum_{\alpha_p}|\alpha_p\rangle\langle\alpha_p| = \sum_{\alpha_p} P^+(\alpha_p)|0\rangle\langle 0|P(\alpha_p) = I, \tag{11}$$

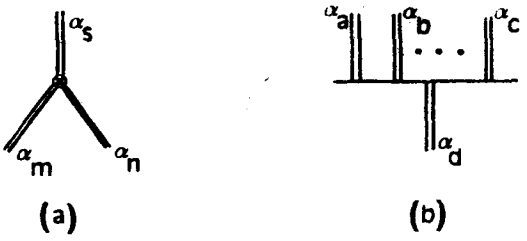

Fig. 5. (a) The vertex $Y^*(\alpha_m\alpha_n;\alpha_s)$. (b) The vertex $\langle\alpha_d|P^+(\alpha_a)P^+(\alpha_b)\ldots P^+(\alpha_c)|0\rangle^*$. The number of particles must be conserved, thus $d = a+b+\ldots+c$.

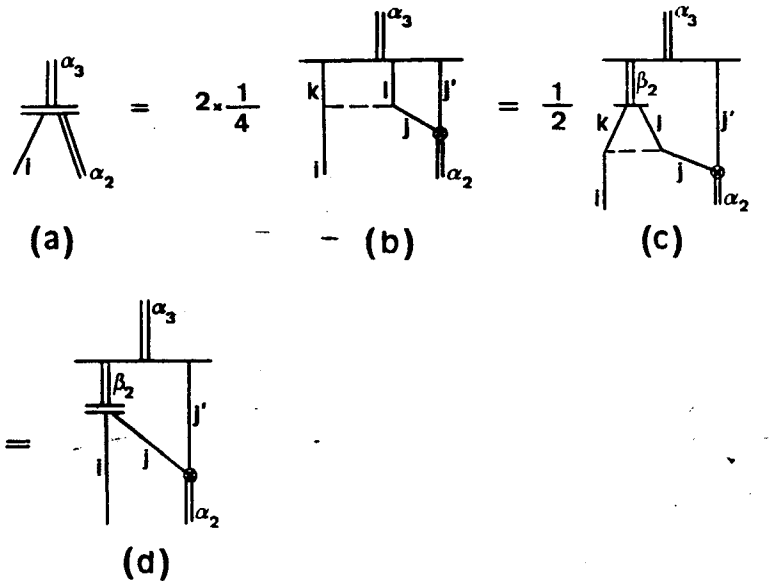

Fig. 6. (a) Coupling constant $\Lambda(i\alpha_2;\alpha_3)$. (b) The block α_2 is open into its single-particle components. One of these components is joined through the interaction with the basis single-particle line. There are two possibilities to do this and both of them give the same graph, thus the factor 2. The factor $\frac{1}{4}$ is given by the interaction ($\frac{1}{2}$) and the crossed vertex ($\frac{1}{2}$). The one-bar vertex represents the overlap $\langle\alpha_3|c_k^+c_i^+c_{j'}^+|0\rangle$. (c) A projector $\sum_{\beta_2}|\beta_2\rangle\langle\beta_2| = I$ is included between two single-particle lines. The one-bar vertices represent $F(kl;\beta_2)$ and $F(\beta_2 j';\alpha_3)$. (d) The coupling constant of fig. 4 is introduced.

one obtains

$$\langle\alpha_3|c_{j'}^+c_k^+c_i^+|0\rangle = \sum_{\beta_2}\langle\alpha_3|c_{j'}^+|\beta_2\rangle\langle\beta_2|c_k^+c_i^+|0\rangle, \tag{12}$$

which is the replacement done in fig. 6c. Finally, one can introduce the two-particle coupling constant given in eq. (9), as represented in fig. 6d, to get [see eq. (8)]

$$(W_{\alpha_3}-\varepsilon_i-\omega_{\alpha_2})F(i\alpha_2;\alpha_3) = \sum_{jj'\beta_2} X(jj';\alpha_2)\Lambda(ij;\beta_2)F(j'\beta_2;\alpha_3), \tag{13}$$

which is the three-particle MSM dynamical equation. One can diagonalize (13) using the usual normalization condition (i.e. the sum of squares equal to one) to obtain the energies W_{α_3} and the overlaps F. But since the basis is not orthogonal, the values of F so calculated are not very meaningful. Yet the energies W_{α_3} agree with the shell-model energies, although a number of spurious states also appear [9, 9]).

As may be noted, in fig. 6 we take the crossed circle as being the amplitude X directly. This is possible because $X(ii;\alpha_2) = 0$. In addition, we have used in eq. (13) the relation $F(j'\beta_2;\alpha_3) = F(\beta_2 j';\alpha_3)$.

Summation runs over all intermediate states in fig. 6 (and the rest of the figures in this paper) although we do not indicate this explicitly in the graph.

The introduction of the pairing coupling constant in fig. 6d was possible due to

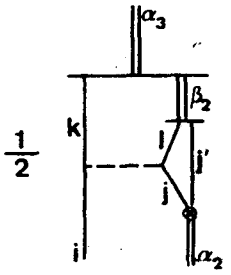

Fig. 7. A way to write the graphs 6b which does not allow us to introduce the coupling constant of fig. 4.

the position in which the projector (line β_2) was placed. In fig. 7 that projector was placed in such a way that no further simplification is possible. In general, the graph makes it apparent where the projector must be positioned in order to replace a part of the graph by a coupling constant. Some important properties of the graphical representation of projectors are found in the appendix.

The graphical evaluation of any coupling constant can be carried out as done for the three-particle case above. However, one does not need to go through all the details and steps of fig. 6 in a more complicated case. In fact, the graphical calculation of the general coupling constant $\Lambda(\alpha_m\alpha_n; \alpha_s)$ is a rather simple task, as seen in fig. 8 First one opens a block – α_n, say, as in fig. 8 – into its two components. Since the interaction only acts among components of different blocks, there are only two contributions. One can then introduce a projector, as in fig. 9, to replace the bare interaction by a coupling constant (fig. 10). To obtain the MSM dynamical equation from fig. 10, one has generally to transform one or more of the lines α_p and α_b in fig. 10b (or α_p and α_a in fig. 10c) into lines that bring the last states back to basis states. In other words, the last blocks in fig. 10b must be partitioned such that $p = m$ (or n) and $b = n$ (or m). Similarly, in fig. 10c it must be $p = m$ (or n) and $a = n$ (or m).

As an illustration, let us consider the case $m = 2$, $n \geqq 4$ and even. In addition,

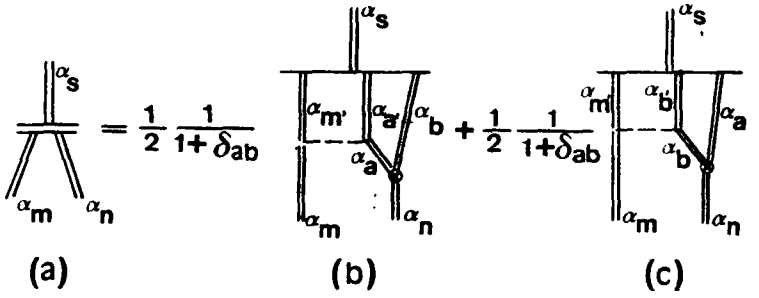

Fig. 8. Graphical evaluation of the general coupling constant $\Lambda(\alpha_m\alpha_n; \alpha_s)$. The factor $\frac{1}{2}$ in (b) and (c) is due to the interaction and the factor $(1+\delta_{ab})^{-1}$ is provided by the crossed circle vertex. The dashed line is supposed to join single-particle lines of the blocks α_m and α_a (or α_b) in (b) [or (c)].

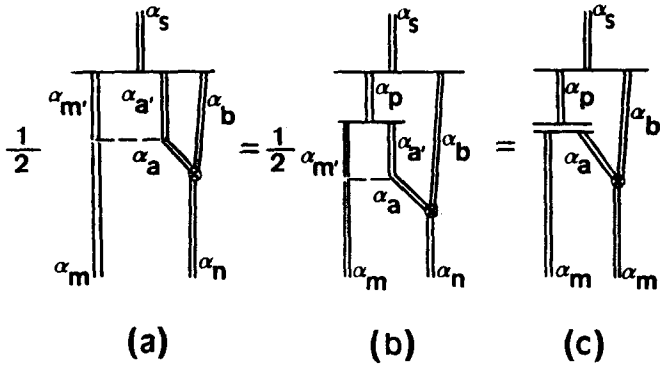

Fig 9. The general graph (a) contains the bare two-particle interaction. In (b) the line α_p (projector) is introduced to replace, in (c), the bare interaction by a coupling constant.

let us assume that all intermediate blocks are also partitioned such that one of these partitions is a two-particle state. This would correspond to set $a = n-2$, $b = 2$ (or vice versa) in fig. 10. Within this partition of the block n, one finds that fig. 10b is already in the MSM final form, while the state α_p ($p = 4$) in fig. 10c must be open once to obtain the diagram 11c.

There are many other possibiliies for the coupling constant of fig. 11. For instance, in the diagram 11c the block α_{n-2} can be opened before the block α_4. One can then follow a number of procedures, one of which can be found in fig. 3c of ref. [14]).

The MSM dynamical equation is, from fig. 11 (using $F(\alpha'_2\alpha'_n;\alpha_s) = F(\alpha'_n\alpha'_2;\alpha_s)$),

$$(W_{\alpha_a} - \omega_{\alpha_2} - W_{\alpha_n})F(\alpha_2\alpha_n;\alpha_s) = \frac{1}{1+\delta_{n4}} \sum_{\alpha'_2\alpha'_n} \Bigg\{ \sum_{\alpha_{n-2}} Y(\alpha_{n-2}\alpha'_2;\alpha_n)\Lambda(\alpha_2\alpha_{n-2};\alpha'_n) \cdot$$

$$+\tfrac{1}{2} \sum_{\beta_2\beta'_2\alpha_4\alpha_{n-2}} Y(\beta_2\alpha_{n-2};\alpha_n)\Lambda(\alpha_2\beta_2;\alpha_4)Y(\alpha'_2\beta'_2;\alpha_4)F(\beta'_2\alpha_{n-2};\alpha'_n)\Bigg\} F(\alpha'_2\alpha'_n;\alpha_s). \quad (14)$$

This equation is actually much more simple than the one that would be obtained from

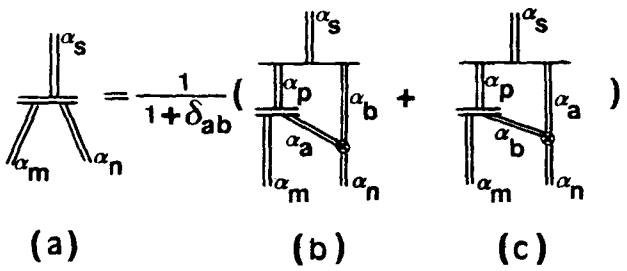

Fig. 10. Graphical expression of the coupling constant $\Lambda(\alpha_m\alpha_n;\alpha_s)$ in terms of intermediate coupling constants. The graphs (a), (b) and (c) are the same as the corresponding ones in fig. 8.

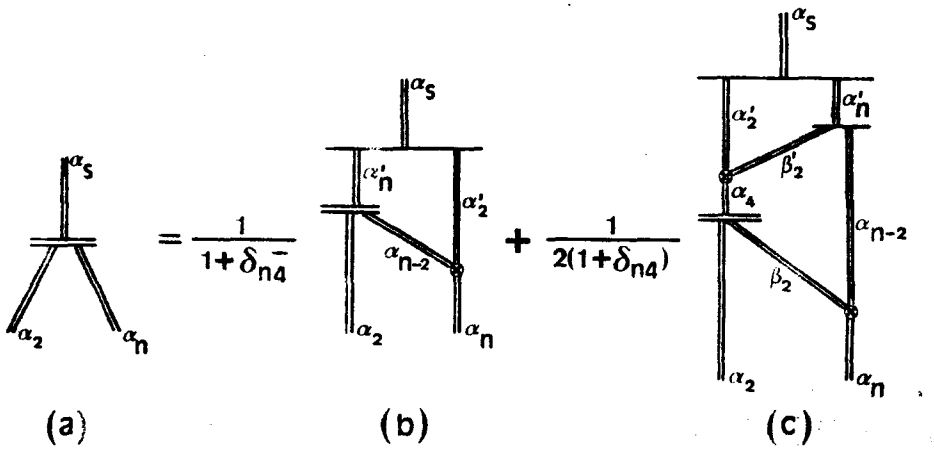

Fig. 11. A MSM graphical equation corresponding to the coupling constant $A(\alpha,\alpha_n;\alpha_s)$. The factor $\frac{1}{2}$ in (c) arises from the crossed circle vertex that opens the line α_4.

fig. 3 of ref. [14]). The special case $n = 4$ can be treated separately. As shown in the appendix, the line α'_n in fig. 11c can be eliminated such that the three lines α'_2, β'_2 and α_{n-2} join the one-bar vertex with α_s. Then, the lines α'_2 and β'_2 can be joined (fig. A3) to obtain a graph which is exactly the same as the graph 11b. Therefore, the factor $1/(1+\delta_{n4})$ is cancelled and one obtains the simple expression of ref. [10]).

To finish this subsection, we point out that when in a graph two lines with odd numbers of particles are crossed, a minus sign must be added. This is due to the fact that in such a case an odd number of single-particle permutations has been done in the commutator of eq. (7). A similar feature is found in the usual graphical treatment of many-body systems. In this case, one sometimes referred to "odd number of closed loops" in the Feynman diagram [24]). In our case, we may have fermion and boson lines interwoven in such a way that to an odd number of loops may not correspond a minus sign.

2.3 METRIC MATRIX

To correct the violations of the Pauli principle as well as the redundancies of the base (1), one must evaluate the metric matrix, which is a special case of the overlap matrix D [cf. (A.4)]; i.e.

$$D(\beta_m\beta_n;\alpha_m\alpha_n) = \langle 0|P(\beta_n)P(\beta_m)P^+(\alpha_m)P^+(\alpha_n)|0\rangle. \tag{15}$$

As for the coupling constant (6), one can write

$$D(\beta_m\beta_n,\alpha_m\alpha_n) = \delta_{\alpha_m\beta_m}\delta_{\alpha_n\beta_n} \pm \delta_{mn}\delta_{\alpha_m\beta_n}\delta_{\alpha_n\beta_m} + C(\beta_m\beta_n,\alpha_m\alpha_n), \tag{16}$$

where

$$C(\beta_m\beta_n,\alpha_m\alpha_n) = \langle\beta_n|[[P(\beta_m),P^+(\alpha_m)]_\mp,P^+(\alpha_n)] \tag{17a}$$

for $m \geqq n$. If $m < n$ one gets

$$C(\beta_m\beta_n, \alpha_m\alpha_n) = \langle\beta_n|[[P(\beta_m), P^+(\alpha_m)]_\mp, P^+(\alpha_n)]|0\rangle \mp \langle\beta_n|P^+(\alpha_m)[P(\beta_m), P^+(\alpha_n)]|0\rangle, \tag{17b}$$

as can easily be verified expanding the double commutator. In eqs. (16)–(17) the upper (lower) sign applies when m is even (odd).

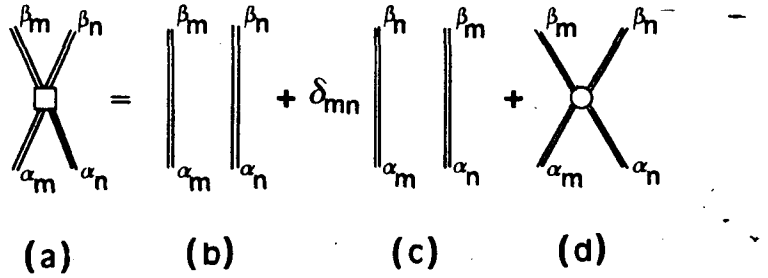

Fig. 12. Graphical representation of the metric matrix eq. (16). The "coin" vertex (d) corresponds to eq. (17).

In fig. 12 we give the graphical representation of eq. (16). The square vertex representing the overlap D is defined in fig. A4. The contribution (17), which does not contain the diagonal part, is represented by a circle vertex. Just to avoid confusion with the crossed circle vertex of fig. 2, we call the vertex 12d "coin" vertex (the form of the vertex justifies the name). This coin vertex represents the correction to the Pauli principle violations in the basis (1).

The reader may wonder whether it is really necessary to introduce so many vertices. In fact, only the coupling constant and the crossed circle vertices would have different meaning within an orthonormal basis. In particular, the coin vertex would be zero in this case. Actually, in theories that use graphical methods and orthonormal bases (as the nuclear field theory), it is the coupling constant that opens or closes lines. But in our case, all the vertices introduced are (in general) independent of each other. They are necessary to express otherwise complicated graphs in a simple form.

The graphical evaluation of eq. (17) can be performed opening the blocks α_m, α_n and β_m up to the single-particle lines. Afterwards *all lines belonging to* β_m must be joined *with all lines* belonging to α_m and α_n. The only graphs that must be disregarded are those in which all lines of α_m (or α_n) remain untouched. These graphs have already been counted in the graphs 12b or 12c.

As for the coupling constant graphs, the diagram itself makes it apparent which of its parts can best be replaced by coin vertices. The continuation of the remaining lines (those which have not been joined) can freely be performed in order to achieve this replacement.

We will illustrate the graphical evaluation of the coin vertex in fig. 12d, analysing the case $m = 2$, $n > 4$ of fig. 11. Thus, in fig. 13 we open the blocks β_2 and α_n into their components. The next step would be to open the lines α_2, γ_2, γ_{n-2} and so on.

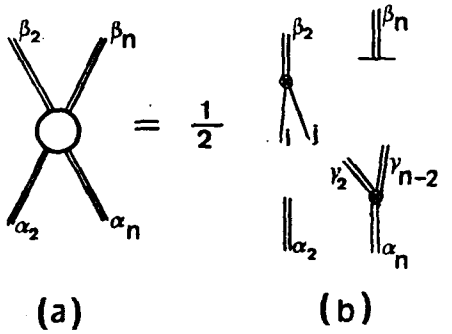

Fig. 13. First operation required to evaluate the coin vertex (a). Since $n > 4$, no factor $\frac{1}{2}$ accompanies the crossed vertex that opens the line α_n.

However, we know that the lines i and j must be continued in such a way that only one of them, at most, is joined to the line α_2. We show in fig. 14 the case in which $i(j)$ joins α_2 and $j(i)$ joins γ_2. In fig. 15 we give the other possibilities. However, the sum of the diagrams in fig. 15 would count twice the contribution in which both i and j join the line γ_{n-2}. This particular case is written in fig. 16. The graphs 15c and 16b can be simplified using the identity shown in fig. A2. Therefore, the coin vertex of fig. 13a is the sum of the graphs 14c plus all graphs in fig. 15 *minus* the graphs in fig. 16. This sum is graphically given in fig. 17, where fig. A2 was used. One can finally write, corresponding to the graphs in fig. 17,

$$
\begin{aligned}
C(\beta_2\beta_n;\alpha_2\alpha_n) = & \sum_{\gamma_2\alpha_{n-2}} Y(\gamma_2\alpha_{n-2};\alpha_n) \\
& \times \Bigg\{ \sum_{\beta_{n-2}} C(\beta_2\beta_{n-2};\alpha_2\alpha_{n-2}) F(\gamma_2\beta_{n-2};\beta_n) \\
& + \sum_{\delta_2} C(\beta_2\delta_2;\alpha_2\gamma_2) F(\delta_2\alpha_{n-2};\beta_n) \\
& - \sum_{\alpha_{n-4}\beta_{n-2}} F^*(\beta_2\alpha_{n-4};\alpha_{n-2}) F(\alpha_2\alpha_{n-4};\beta_{n-2}) F(\gamma_2\beta_{n-2};\beta_n) \Bigg\} \\
& + \sum_{\alpha_{n-2}} F^*(\beta_2\alpha_{n-2};\alpha_n) F(\alpha_2\alpha_{n-2};\beta_n); \qquad (18)
\end{aligned}
$$

we have freely used the equality $F(\alpha_a\alpha_b;\alpha_c) = F(\alpha_b\alpha_a;\alpha_c)$ and similarly for the amplitude Y. This property is valid here because both a and b are even numbers.

An important feature of the example discussed above, is that we found closed formulas for both the dynamical and the metric matrices (eqs. (14) and (18), respectively). From a practical view point, this suggests that it may pay to construct a good computer code which would then be of a general use.

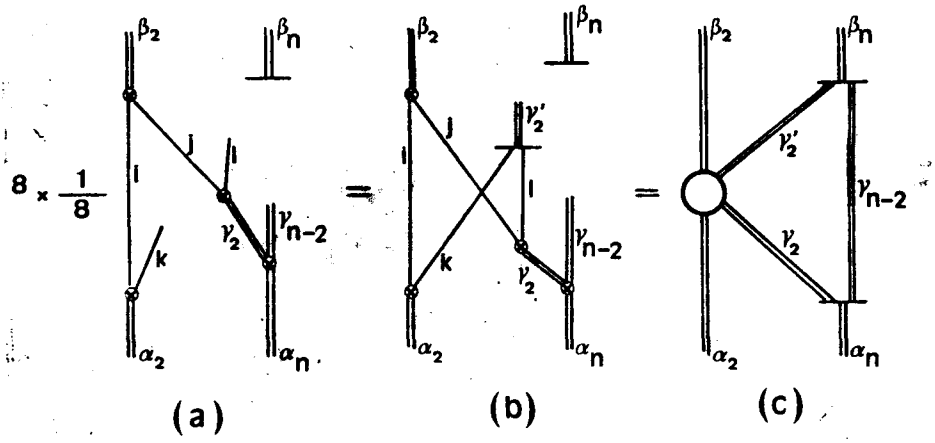

Fig. 14. (a) The lines i and j join lines belonging to the blocks α_2 and γ_2. There are 8 different ways in which this can be achieved, all of them giving the same contribution. (b) A projector (line γ_2') is placed to allow the introduction of a coin vertex. The crossing of the lines j and k indicates that a minus sign should be added to the analytical expression. (c) A coin vertex is introduced and with it all the factors (including the minus sign) that appear in the quantity $C(\beta_2\gamma_2', \alpha_2\gamma_2)$ [eq. (17)].

Similar close formulas can be found for other partitions and systems. In particular, there are equations which are formally simpler than (14) and (18) to describe any system within partitions in which $m = 1$, as the interested reader may find himself or ask us for details. In the next section, some other cases will be partially analysed.

In the example above, we assumed the block β_n to be inert. Equations which are completely different to eq. (18) can be obtained if one assumes the two-particle block β_2 to be inert. In this case, however, even the graphical calculation becomes cumbersome, because there are too many active single-particle lines to be joined. Moreover, for some graphs it may not be possible to introduce coin vertices. In fig. 18 we show

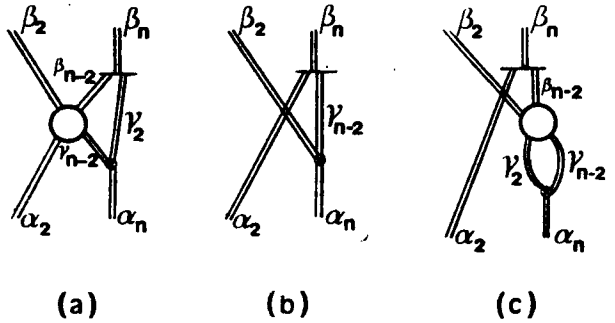

Fig. 15. Contributions to the coin vertex of fig. 13 (see fig. 13b). (a) This graph gives two contributions: (i) The two lines of β_2 join γ_{n-2}. (ii) One line of β_2 joins α_2 and the other γ_{n-2}. (b) Both lines of β_2 join γ_2. This contribution corresponds to the second term in the r.h.s. of eq. (17b). (c) Also this graph gives two contributions: (i) The two lines of β_2 join γ_{n-2}. (ii) One line of β_2 joins γ_2 and the other γ_{n-2}. When summing these three graphs, the contribution in which the two lines of β_2 join γ_{n-2} has been counted twice.

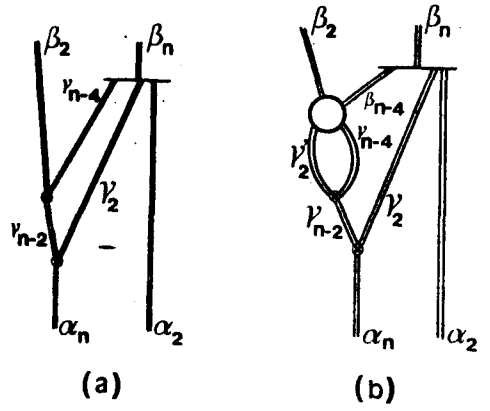

Fig. 16. The line γ_{n-2} of fig. 13 is open into the two-particle line γ_2' and the $n-4$ particle line γ_{n-4}. (a) The two lines of β_2 join γ_2'. (b) There are two contributions: (i) Both lines of β_2 join γ_{n-4}; (ii) One line of β_2 joins γ_2' and the other γ_{n-4}. The sum of these two graphs is the contribution to fig. 15 in which both lines of β_2 join γ_{n-2}.

such a graph corresponding to a six-particle system. Since no simplifications have been carried out in fig. 18 (i.e. neither a coin vertex nor any other MSM vertex could have been introduced) the corresponding analytical expression is rather complicated. In particular, there would be high-order angular momentum recoupling coefficients

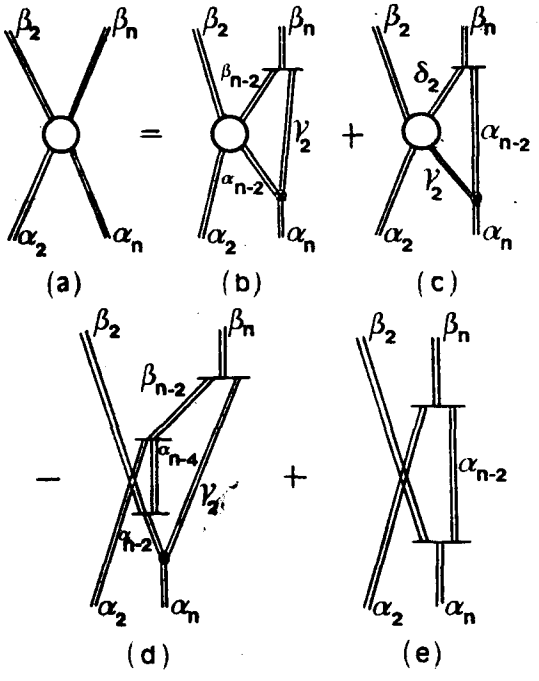

Fig. 17. Graphical equation for the coin vertex $C(\beta_2\beta_n; \alpha_2\alpha_n)$ for [illegible] and even.

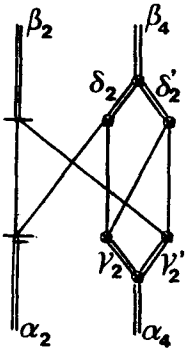

Fig. 18. A contribution to the metric matrix $D(\beta_2\beta_4; \alpha_2\alpha_4)$ corresponding to the case in which the line β_2 is the inert block.

(a product of seven 6-j symbols, in fact). This complicated contribution may be compared with the relatively simple expression found in ref. [10]).

2.4. TRANSITION OPERATOR MATRIX ELEMENTS

In this subsection we will analyse the MSM graphical evaluation of electromagnetic transition matrix element and one- and two-particle transfer form factors.

The electromagnetic transition operator can be written as

$$M = \sum_{ij} \langle i|M|j\rangle c_i^+ c_j, \tag{19}$$

and the corresponding MSM matrix elements are

$$\langle \beta_s|M|\alpha_s\rangle = \frac{1}{1+\delta_{mn}} \sum_{\alpha_m\alpha_n} Y(\alpha_m\alpha_n; \alpha_s)\langle \beta_s|[M, P^+(\alpha_m)P^+(\alpha_n)]|0\rangle. \tag{20}$$

Since M is a one-particle operator, the graphical representation of eq. (20) is very simple, as seen in fig. 19. The operator M acts upon a particle belonging either to

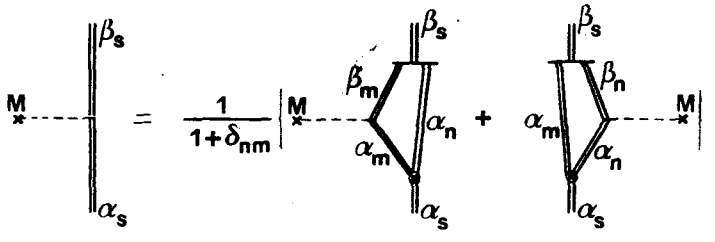

Fig. 19. Graphical representation of electromagnetic transition matrix elements.

the block α_m or α_n. Since after that operation the remaining lines can be continued as one wishes, the most convenient way to proceed with these lines is to return to the original partitions. One therefore obtains, from fig. 19,

$$\langle\beta_s|M|\alpha_s\rangle = \frac{1}{1+\delta_{nm}} \sum_{\alpha_n\alpha_m} Y(\alpha_m\alpha_n;\alpha_s)\Bigg[\sum_{\beta_m}\langle\beta_m|M|\alpha_m\rangle F(\beta_m\alpha_n;\beta_s) + \sum_{\beta_n}\langle\beta_n|M|\alpha_n\rangle F(\alpha_m\beta_n;\beta_s)\Bigg]. \quad (21)$$

An important feature of this equation is that it predicts that for pure states (i.e. only one value of Y is relevant, as would be the case for vibrational states) the collectivity of the states α_s (β_s are ground states) remains rather unchanged with the number of particles s.

The one- and two-particle transfer form factors are actually by-products of the MSM [9, 10]). For the one-particle case one has

$$t(i) = \langle\alpha_s|c_i^+|0\rangle, \quad (22)$$

where $|0\rangle$ is the target ground state. Using a partition of the final system, such that $m = 1$; n even, one has from eq. (5)

$$t(i) = F(i\alpha_n^0;\alpha_s), \quad (23)$$

where α_n^0 labels the n-particle ground state.

In the same fashion, the two-particle form factor is

$$f(ij;\alpha_s) = \langle\alpha_s|c_i^+c_j^+|0\rangle/(1+\delta_{ij}), \quad (24)$$

where, as before, $|0\rangle$ is the target ground state. From eq. (2) and since the two-particle basis is orthogonal, one gets

$$f(ij;\alpha_s) = \sum_{\alpha_2} X^*(ij;\alpha_2)\langle\alpha_s|P^+(\alpha_2)|0\rangle. \quad (25)$$

Using the partition $m = 2$; n even, one finally obtains

$$f(ij;\alpha_s) = \sum_{\alpha_2} X^*(ij;\alpha_2)F(\alpha_2\alpha_n^0;\alpha_s). \quad (26)$$

A final comment on the angular momentum coupling: All the graphs shown in this section are well suited to use a graphical method to couple angular momenta [25–27]). Moreover, different procedures to build a given graph may give different angular momentum coupling coefficients. Using also a graphical procedure to couple angular momenta, one may quickly decide which graph is the simplest among all those possibilities. This can be done because in the MSM diagrams, reducible graphs [26]) are easy to recognize.

3. Applications

The graph in fig. 18 is an example of the difficulties inherent to any description which uses only single-particle variables as elementary degrees of freedom. The number of configurations soon becomes large and, consequently, to solve relatively simple systems like the one in fig. 18 requires complex calculations. As a counterpart, within the MSM the six-particle system can be solved very economically. If one proceeds as in fig. 17, only the graphs 17c and 17e are present for $n = 4$. Of these two graphs, the most difficult is 17c, which includes only two six-j symbols [10]. Although these features are very important from the point of view of the calculations, there are also some physical consequences emerging from the interrelation among the MSM vertices, their constituent states, and the rest of the states in a given diagram. For instance, one may wonder whether all coin vertices are necessary to calculate a given diagram. Perhaps there are only relatively few coin vertices which are relevant and the rest may be disregarded. The same can naturally be said of the other MSM vertices. This question may touch another important subject, namely the connection between nuclear collective motion and the single-particle components of the collective degrees of freedom. Although we do not intend to analyse this question here, it is worthwhile to point out that the success of the interacting boson model [7] (IBM) may justify such an analysis. Actually, recent schematic calculations tend to indicate that the IBM is a truncation scheme for shell-model calculations [see e.g. refs. [38-41]]. However, the relation between single-particle and collective degrees of freedom in real nuclei is a subject which remains largely unexplored, partly due to the calculation difficulties encountered when dealing with many-body systems. Only recently have realistic microscopic calculations been carried out trying to explain rotational-like spectra, and then within rather few single-particle states [28, 29]. In fact, a full microscopic calculation for a many-nucleon system, which would introduce the nucleon-nucleon interaction from the outset, does not seem to be feasible in heavy and medium nuclei. For instance, considering only six single-hole (neutron) states in ^{208}Pb, as usual [10], there are 6 states 0^+ in ^{206}Pb, 2411 in ^{202}Pb, 413863 in ^{198}Pb and about 10^8 in ^{194}Pb. We made a computer code to count those shell-model states †. *Only the counting* of all states in ^{198}Pb took more than 10 hours of CPU time in a PDP 11/70 computer! Clearly, one cannot escape making, at least, drastic truncations of the shell-model basis if many-nucleon systems are ever to be analyzed within the shell-model. But the shell-model is not well suited to reduce even further its dimensions, because the pairing interaction is so strong that shell-model configurations that are very distant (in energy) from each other may have similar importance to describe physical states. Yet, the shell-model single-particle vectors span a very small subspace of the total Hilbert space. Actually, one of the great features of the

† We are indebted to Jan Blomqvist for discussions on economical procedures to count shell-model states.

shell model is that it provides a very effective representation to describe physical states. In this sense, the shell model is not "a model" but a good starting point to solve the many-body Schroedinger equation in nuclei.

It is precisely to carry on additional truncations to the shell-model basis that methods and models that include correlated states in the basis were introduced. In particular, it was recently shown that most physical states in ^{204}Pb and ^{202}Pb are contained in very small MSM subspaces [10]). The ground states in both nuclei are practically proportional to only one MSM basis element, namely

$$|\text{g.s.}; s\rangle = N_s P^+(\text{g.s.}; 2) P^+(\text{g.s.}; n)|0\rangle, \tag{27}$$

where the partition $m = 2$ was used. A reason why within correlated bases the physical states are so "pure", is that the pairing interaction is already included in the basis. As a consequence, the "energy criterion" to choose basis elements works well, i.e. only basis states which are close (in energy) to the physical vectors are relevant [10, 31]). This feature is confirmed by the "purity" of ground states, as described by the MSM, since the basis element (27) is isolated from the rest of the MSM basis states. If the energy criterion to truncate the MSM basis proves to be valid for any number of particles outside the core, one may hope to describe microscopically at least some of the collective features in intermediate and rotational nuclei, as suggested by the IBM.

In this section we will apply the MSM equations derived previously to cases where only very few basis states, as the ground state in eq. (27), are important to describe physical vectors.

We will first analyse nuclei with only one kind of particle (neutrons or protons) outside magic cores. The partition to be used is in this case $m = 2$, $n =$ even as in eq. (14). This equation should be coupled to good angular momenta, a procedure that may be carried out graphically directly from fig. 11, or analytically from eq. (14), since this is a simple case. To the first term on the right-hand side of eq. (14) a 6-j symbol should be added, while there are two 6-j symbols to be added to the second term. However, in the cases to be analysed below, at least one of the states in the MSM basis will have zero angular momentum and no additional factor appears in (14).

3.1. TWO-PARTICLE (PAIRING) CONTRIBUTION TO GROUND STATES

Introducing the approximation (27) into eq. (14), one obtains

$$W_{\alpha_s} = W^{(0)}_{\alpha_s} + W^{(1)}_{\alpha_s} + W^{(2)}_{\alpha_s}, \tag{28a}$$

where

$$W^{(0)}_{\alpha_s} = \omega_{\alpha_2} + W_{\alpha_n}, \tag{28b}$$

$$W^{(1)}_{\alpha_s} = W_{\alpha_n} - \omega_{\alpha_2} - W_{\alpha_{n-2}}, \tag{28c}$$

$$W^{(2)}_{\alpha_s} = W_{\alpha_4} - 2W_{\alpha_2}, \tag{28d}$$

and α_m labels the ground state of the m-particle nucleus. To derive eq. (28) the orthonormality relation (3) was used, which in this case reads $X(\alpha_2\alpha_p;\alpha_q)F(\alpha_2\alpha_p;\alpha_q) = 1$. This equation implies that all cross vertices in fig. 11 are cancelled by the corresponding one-bar vertices, except the vertex which opens α_4 in fig. 11c. Only for this vertex does eq. (2.3) give a factor 2 which is cancelled by the factor $\frac{1}{2}$ in fig. 11c.

Eq. (28) gives the ground-state energy of $\frac{1}{2}s$ pairs of nucleons outside a magic core. This is a multiphonon state within the pairing vibration model. Actually, within this model a series of nuclei has already been analysed around closed-shell cores [32, 33]. It was then found that two-particle transfer reactions among members of the pairing multiplet follow qualitatively the pairing model. The energy of the corresponding states, however, is not well predicted by the harmonic pairing model. This energy would simply be $W_{\alpha_s} = \frac{1}{2}s\omega_{\alpha_s}$ [notation as in eq. (28)], which is well beyond the experimental value. A more reasonable value for that energy would be the zero-order energy $W^{(0)}_{\alpha_s}$. Still, the difference between this and the experimental values is generally of the order of several MeV.

In our method we apply eq. (28), but in a given step we take the energies of the previous steps as given by experiment. This "renormalization" procedure was already discussed in the section above. Since the experimental binding energies are known within a certain error [34], we wrote (28) in terms of the binding energies and calculated the corresponding propagated error. Many of the "experimental" values are taken from systematics, in which case large errors (up to 1 MeV) may be encountered [34]. As shown in ref. [14]), in the lead and tin regions eq. (28) gives a good description of the experimental data. In that reference, only neutron excitations were given. In table 1 we give the proton excitations in the same regions. The few ground-state energies known around ^{208}Pb, i.e. ^{214}Ra and ^{216}Th, are well given by eq. (28). In tin, however, the agreement between theory and experiment is not so good. Although rather large experimental errors are found in table 1a, the departure of about 850 keV for the calculated ground-state energy of $^{150}_{68}$Er with respect to experiment, may indicate that this nucleus is deformed, since around $^{146}_{64}$Gd deformations set in very fast. In this case other MSM components (mainly quadrupole states, probably) may become important. Yet, this is not a clear-cut example of a rotational nucleus (as other cases to be analysed below). One has to consider the large difference between the experimental energies and the corresponding zero order values in table 1a. The contribution $W^{(1)}_{\alpha_s} + W^{(2)}_{\alpha_s}$ is about -17 MeV in ^{150}Er. This number is high enough to make the 850 keV mentioned above a rather small quantity, and all $N = 82$ nuclei seem to be spherical. In fact, $^{146}_{64}$Gd is spherical [36], although ^{152}Gd is already deformed.

The departure from experimental values in all the cases in table 1, may actually indicate that other MSM vectors are strongly overlapping with the vector (27). In ^{202}Pb, for instance, the ground-state energy calculated from eq. (28) is wrong by about 300 keV. But already with a two-dimensional basis that energy is within 60 keV in agreement with the experimental value [10]. Within a four-dimensional basis, one is

TABLE 1

Calculated and experimental [34]) ground-state energies (in MeV) for pairs of protons outside magic cores in the tin (a) and lead (b) regions

	(a) $N = 82$, $Z = 50+n$				(b) $N = 126$, $Z = 82+n$			
n	$W^{(0)}$	$W^{(1)}$	W (theor.)	W (exp.)	$W^{(0)}$	$W^{(1)}$	W (theor.)	W (exp.)
6	60.05	−2.53	54.99	55.62	24.84	−1.50	21.84	21.89
8	76.48	−4.43	69.51	70.00	30.67	−2.96	26.21	26.16
10	90.86	−6.47	81.86	82.45	34.94	−4.51	28.93	
12	103.31	−8.41	92.36	93.04				
14	113.90	−10.27	101.11	101.57				
16	112.43	−12.33	107.57	108.00				
18	128.86	−14.43	111.90	112.75				
20	133.61	−16.11	114.97					

The number of protons is n. The zero-order contribution $W^{(0)}$ and the contribution $W^{(1)}$ are from eqs. (28b) and (28c), respectively. The contribution $W^{(2)}$ [eq. (28d)] is −2.35 MeV in tin and −1.50 MeV in lead. The experimental values in tin are accompanied by rather large experimental errors. They go from 0.23 MeV in $^{144}_{62}$Sm ($n = 12$) to 0.51 MeV in $^{150}_{68}$Er ($n = 18$). To estimate these errors we assumed an experimental error of 100 keV for those binding energies taken from systematics, which actually may reach up to 1 MeV [ref. [34])].

right over the experimental energy, although such an exceptional agreement may be accidental.

The important point here is that the ^{202}Pb ground state practically coincides with the state (27), irrespective of the dimension of the basis. But the angle θ between the vector (27) and the second basis vector is such that $\cos\theta = 0.95$ and these vectors are nearly parallel. A similar feature may be present in all cases calculated in this section.

The reasonable agreement between theory and experiment found above for neutron and proton pairs suggests that the approximation (27) may be valid for a more general case, namely where both kinds of pairs are mixed. To analyse this point we consider the simple situation in which one kind of pair (neutron or proton) is placed outside the core and then pairs of the other kind are added. In the following we refer to a proton pair and many neutron pairs, but the derivations are, of course, also valid for the inverse situation. After the proton pair has been added to the core, we assume that the two-proton isotopes are described by the MSM wave function (27), where P^+(g.s.; 2) is the neutron pair creation operator and P^+(g.s.; n) creates the 2 proton plus (n–2) neutron ground state. The ground-state energy W_{α_n} can be obtained directly from fig. 11, as before. Therefore, eq. (28) remains valid with α_2 and α_4 as neutron states, while α_n and α_{n-2} contain a proton pair.

In tables 2 and 3 we present the corresponding ground-state energies in the lead and tin regions. Again here the agreement between theory and experiment is good enough to assume that the approximation (27) is valid. In particular, note that the changing of sign of $W^{(1)}_{2_n}$ in table 2a is necessary for approaching the right final

TABLE 2

Calculated and experimental ground-state energies (see caption table 1)

(a)					(b)				
$_{80}$Hg isotopes					$N = 124$ isotones				
N	$W^{(0)}$	$W^{(1)}$	W (theor.)	W (exp.)	Z	$W^{(0)}$	$W^{(1)}$	W (theor.)	W (exp.)
122	−41.88	1.71	−40.89	−41.27	86	2.93	−0.52	0.91	0.86
120	−55.37	0.62	−55.47	−55.25	88	9.64	−2.07	6.07	5.94
118	−69.36	0.12	−69.95	−69.94	90	14.72	−3.70	9.52	9.54
116	−84.05	−0.59	−85.35	−85.20	92	18.32	−5.18	11.64	
114	−99.31	−1.15	−101.18	−100.99					
112	−115.09	−1.68	−117.48	−117.37					
110	−131.48	−2.28	−134.47	−134.52					
108	−148.63	−3.04	−552.38	−151.74					
106	−165.85	−3.11	−169.67	−169.42					
104	−183.53	−3.57	−187.81	−187.87					
102	−201.98	−4.34	−207.03	−206.84					
100	−220.95	−4.86	−226.52	−226.33					
98	−240.44	−5.38	−246.53	−246.41					
96	−260.52	−5.97	−267.20						

(a) A proton pair hole in the ^{208}Pb core plus neutron pair holes. The total number of neutrons is N. The contribution $W^{(2)}$ is −0.71 MeV.

(b) A neutron pair hole in the ^{208}Pb core plus proton pair particles. The total number of protons is Z. The contribution $W^{(2)}$ is −1.50 MeV.

TABLE 3

As table 2a with ^{132}Sn as a core. The contribution $W^{(2)}$ is −0.93 MeV

$_{52}$Te isotopes				
N	$W^{(0)}$	$W^{(1)}$	W (theor.)	W (exp.)
78	−4.89	−1.45	−7.28	−6.75
76	−18.90	−1.86	−21.69	−21.25
74	−33.40	−2.35	−36.68	−36.32
72	−48.47	−2.92	−52.32	−52.01
70	−64.16	−3.54	−68.63	−68.37
68	−80.52	−4.21	−85.65	−85.41
66	−97.56	−4.89	−103.38	−103.28
64	−115.43	−5.73	−122.09	−121.73
62	−133.88	−6.30	−141.11	−141.05
60	−153.20	−7.17	−161.30	−161.83
58	−173.98	−8.63	−183.54	−183.77
56	−195.92	−9.79	−206.64	−206.35
54	−218.50	−10.43	−229.86	

energies. This feature clearly indicates that the good agreement between theory and experiment is not accidental. Note also the big difference between the values W_{α_s} in tables 2a and 2b.

We also calculated a number of other nuclei around closed shell cores and in all cases obtained results similar to those in tables 2 and 3.

3.2. GROUND STATES AS SUPERPOSITIONS OF α-PARTICLES

So far we have only considered partitions in which one of the systems consisted of a pair of particles ($m = 2$). A natural extension would seem to treat $m = 4$ partitions, where the four particles are a neutron- and a proton-pair. This "α-cluster" type of structure is well known in light nuclei [35]), where $N = Z$. We thus assume the ground state of a nucleus with $s = 4 + n$ nucleons outside a magic core as

$$|\text{g.s.}; s\rangle = N_s P^+(\text{g.s.}; 4) P^+(\text{g.s.}; n)|0\rangle, \tag{29}$$

where $P^+(\text{g.s.}; 4)$ creates the ground state of the nucleus with two protons and two neutrons outside the magic core. We call this nucleus the "one α-particle nucleus". Similarly, the operator $P^+(\text{g.s.}; n)$ creates the $\frac{1}{4}n$ α-particle nucleus.

The coupling constant corresponding to eq. (29) is shown in fig. 20. Since here, as was the case in fig. 11, all states have zero units of angular momentum, there is not any angular momentum coupling coefficients and the coupling constant can directly be obtained from fig. 20. This figure is very similar to fig. 11 and all derivations leading to eq. (28) are also valid here. One readily obtains an equation similar to (28a) but with

$$W^{(0)}_{\alpha_s} = W_{\alpha_4} + W_{\alpha_n}, \tag{30a}$$

$$W^{(1)}_{\alpha_s} = W_{\alpha_n} - W_{\alpha_4} - W_{\alpha_{n-4}}, \tag{30b}$$

$$W^{(2)}_{\alpha_s} = W_{\alpha_8} - 2W_{\alpha_4}, \tag{30c}$$

where W_{α_m} labels the ground state of the $\frac{1}{4}m$ α-particle nucleus.

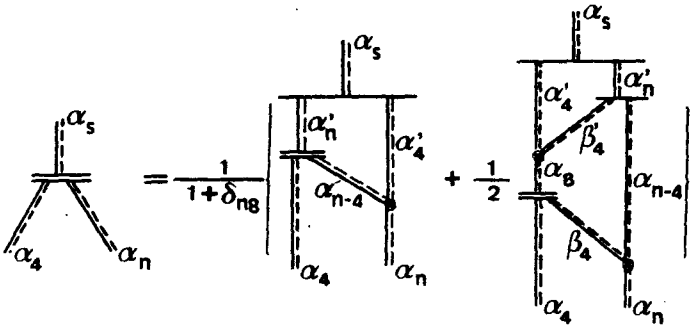

Fig. 20. Coupling constant corresponding to a nucleus with $\frac{1}{4}s$ α-particles outside the magic core. The dashed lines indicate that the corresponding states contain an equal number of neutrons and protons. Thus, α_4 labels a two-proton two-neutron state.

TABLE 4

Ground-state energies (in MeV), eq. (30) for ^{208}Pb as the core

N	Z	$W^{(0)}$	$W^{(1)}$	W (theor.)	W (exp.)	d
132	88	58.78	0.75	60.28	60.14	0.14
134	90	79.48	1.36	81.59	81.13	0.46
136	92	100.48	1.65	102.88	102.62	0.25
138	94	121.97	2.15	124.87	124.20	0.66
140	96	143.55	2.24	146.54	145.40	1.14
142	98	164.74	1.85	167.35	165.98	1.37
144	100	185.32	1.24	187.31		

The numbers N and Z indicate neutron and proton numbers, respectively. The contribution $W_{\alpha_s}^{(2)}$ [eq. (30c)] is here equal to -0.75 MeV. The difference between theoretical and experimental values is d [eq. (31)].

In table 4 we show the calculated ground-state energies corresponding to ^{208}Pb plus α-particle nuclei. This is a good example of the breaking down of a pure MSM description when deformations set in. For spherical nuclei the calculated energies are in good agreement with experimental data. In the well-deformed nuclei (above $A = 228$ in table 4) the contribution $W_{\alpha_s}^{(1)}$ does not increase regularly with A, as for spherical nuclei, and the energy difference between theory and experiment is more than 1 MeV.

A similar effect is seen in the tin region, as shown in table 5. For $A > 148$ one reaches a well-deformed region and the contribution $W_{\alpha_s}^{(1)}$ shows an irregular dependence upon A. Another interesting feature emerging from table 5 is that when one crosses the magic number $Z = 82$, a sudden jump in

$$d = W_{\alpha_s}(\text{theor.}) - W_{\alpha_s}(\text{exp.}) \tag{31}$$

is seen. This is because our MSM states contain only single-particle components belonging to the major shell close to the original magic core. Actually, this feature may help to determine how "magic" is a given number N or Z. For instance, in table 6 we show the calculated ground-state energy corresponding to the core [36] ^{146}Gd minus α-particle nuclei. The same jump seen in table 5 is here found for $Z = 50, N = 68$; $Z = 38$, $N = 56$ and $Z = 32, N = 50$. Strictly speaking, in this case our calculations would only be valid up to $A = 118$, i.e. up to the point where one reaches the end of the original major shell. But the general tendency of the smooth variation of d versus A remains valid irrespective of the point where one stops the MSM process given by eq. (30). Therefore, the abrupt change of $d(A)$ in table 6 does not depend upon our way of calculating W_{α_s}.

It is perhaps not very surprising to find in table 6 that the major shell filling 50 nucleons is so tightly closed. However, the nucleus $^{94}_{38}$Sr was only recently found to be a "magic" nucleus [28, 30], although $^{88}_{38}$Sr was already long ago considered a good hard core [37].

TABLE 5

As table 4 for the ^{132}Sn core; the contribution $W^{(2)}_{a_2}$ is −0.09 MeV

N	Z	$W^{(0)}$	$W^{(1)}$	W (theor.)	W (exp.)	d
88	56	87.39	−0.09	87.21	87.80	−0.59
90	58	116.96	0.41	117.28	117.20	0.08
92	60	146.36	0.24	146.51	147.36	−0.85
94	62	176.52	1.00	177.43	177.30	0.13
96	64	206.46	0.78	207.16	206.60	0.56
98	66	235.76	0.13	235.80	235.34	0.46
100	68	265.50	−0.42	264.00	263.08	0.92
102	70	292.24	−1.42	290.73	290.07	0.66
104	72	319.23	−2.17	316.97	316.11	0.86
106	74	345.27	−3.12	342.05	341.88	0.17
108	76	371.04	−3.38	367.57	367.21	0.36
110	78	396.37	−3.83	392.45	391.49	0.96
112	80	420.65	−4.88	415.68	416.39	−0.71
114	82	445.55	−4.26	441.20	440.29	0.91
116	84	469.45	−5.26	464.10	462.60	1.50
118	86	491.76	−6.85	484.82	484.35	0.47
120	88	513.51	−7.41	506.10	505.38	0.63
122	90	534.54	−8.13	526.32		

TABLE 6

As table 4 for the ^{146}Gd core; the contribution $W^{(2)}_{a_2}$ is −0.01 MeV

N	Z	$W^{(0)}$	$W^{(1)}$	W (theor.)	W (exp.)	d
76	58	−82.99	−0.01	−83.02	−83.31	0.29
74	56	−110.97	−0.32	−111.30	−111.49	0.19
72	54	−139.15	−0.53	−139.69	−140.36	0.66
70	52	−168.02	−1.20	−169.23	−169.94	0.70
68	50	−197.59	−1.92	−199.53	−199.31	−0.22
66	48	−226.96	−1.71	−228.69	−231.66	2.97
64	46	−259.32	−4.70	−264.03	−264.07	0.04
62	44	−291.73	−4.75	−296.49	−296.79	0.30
60	42	−324.45	−5.07	−329.53	−330.28	0.75
58	40	−357.94	−5.83	−363.70	−363.27	−0.51
56	38	−390.93	−5.33	−396.28	−396.32	0.04
54	36	−423.98	−5.39	−429.38	−430.82	1.44
52	34	−458.48	−6.84	−465.33	−465.87	0.54
50	32	−493.53	−7.39	−500.93	−501.66	0.73
48	30	−529.32	−8.13	−537.46	−540.09	2.63
46	28	−567.75	−10.77	−578.53		

Finally, it is worthwhile to point out that a standard shell-model calculation in any of the cases presented in this section would be virtually impossible. As mentioned in the previous section, the shell-model dimensions in the middle of a major shell in medium and heavy nuclei is of the order of hundreds of millions.

4. Summary and conclusions

An important feature of the multistep shell-model method (MSM) is that it allows us to solve the shell-model equations corresponding to a nucleus with many nucleons outside the core in several steps. In each step one calculates a different nucleus using only few states of previously evaluated nuclei. With the energies and wave functions thus calculated, one builds up building blocks that are used in later steps. Since all the algebraical complexities inherent in each block are not passed to the final equations, the MSM formalism turns out to be relatively simple. However, the inclusion of such building blocks in the different steps of the method is not an easy task. Moreover, there might be many different ways to write down the MSM equations and it may not be easy to find the most convinient of those possibilities. To overcome these difficulties, we presented in this paper a graphical procedure to find the MSM equations. Using this procedure, one can readily visualize all those possibilities and, therefore, to quickly decide which is the one that best fits the criterion of formal simplicity or other physical requirements.

We applied this graphical procedure to evaluate the ground-state energies and wave functions of many-nucleon systems using different MSM representations. In all cases we found very simple formulas to calculate binding energies in spherical nuclei. Although in these applications tens of particles outside the core were active, we found that only one MSM configuration was enough to get good agreement with experimental data. But when the number of neutrons or protons crosses a magic number or a deformed region is reached, that agreement becomes suddenly very poor. Therefore, one may use those simple formulas to confirm whether a given nucleus is deformed or a given shell is "magic". Thus, we found that the nucleus $^{94}_{38}Sr_{56}$ may be considered a good hard core, as recently suggested [28, 30].

We also found closed formulas for the different steps of the MSM. It would then be possible to solve the shell-model equations with the same degree of complexity, *irrespective of the number of active particles*. Thus, if drastic truncations are possible in general, as suggested by our present ground-state calculations and previous six-particle calculations in the lead region [10], one may calculate systems for which standard shell-model calculations are impossible today.

One of us (C.P.) would like to express his gratitude towards the Research Institute of Physics, Stockholm, for financial support and excellent working conditions.

Appendix

The orthonormality relation (3) can be represented graphically, as shown in fig. A1. A more general orthonormality relation, useful for evaluating metric matrices, is

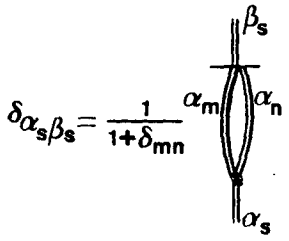

Fig. A1. Graphical representation of the orthonormality relation eq. (3).

given by the identity [the upper (lower) sign applies when b is even (odd)]

$$\sum_{\alpha_a\alpha_b} Y(\alpha_a\alpha_b;\gamma_p)\{\langle 0|P(\beta_b)P(\beta_a)P^+(\alpha_a)P^+(\alpha_b)|0\rangle - \delta_{\alpha_a\beta_a}\delta_{\alpha_b\beta_b} \mp \delta_{ab}\delta_{\alpha_a\beta_b}\delta_{\alpha_b\beta_a}\}$$

$$= (1+\delta_{ab})\{\langle\gamma_p|P^+(\beta_a)P^+(\beta_b)|0\rangle^* - Y(\beta_a\beta_b;\gamma_p)\}, \qquad (A.1)$$

which is represented in fig. A2. In fig. 6 the graphical representation of the projector (11) was introduced. In general, one can put in any projector among lines that *converge* towards a one-bar vertex, as seen in fig. A3. This property stems from the definition of the one-bar vertex, i.e.

$$\langle\alpha_f|P^+(\alpha_a)P^+(\alpha_b)\ldots P^+(\alpha_c)\ldots P^+(\alpha_d)\ldots P^+(\alpha_e)|0\rangle$$

$$= \sum_{\alpha_p}\langle\alpha_f|P^+(\alpha_a)P^+(\alpha_b)\ldots P^+(\alpha_p)\ldots P^+(\alpha_e)|0\rangle\langle\alpha_p|P^+(\alpha_c)\ldots P^+(\alpha_d)|0\rangle, \qquad (A.2)$$

which is the analytical expression corresponding to fig. A3. From this figure, one can see that the inverse property is also valid, i.e., a line confined between one-bar vertices (as the line α_p) can be dropped if there is only one line on the other side of any of the

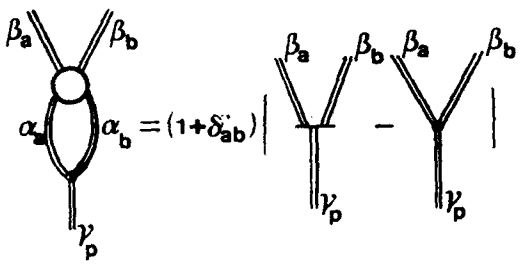

Fig. A2. Graphical representation of the identity (A.1). The circle (coin) vertex is defined in fig. 12.

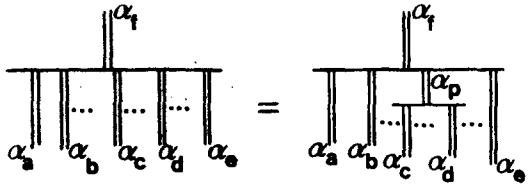

Fig. A3. A projector $\sum_{\alpha_p} |\alpha_p\rangle\langle\alpha_p| = I$ can be introduced among any number of lines which converge towards a one-bar vertex. The only condition is that the number of particles must be conserved, i.e., in the figure $p = c + \ldots + d$.

one-bar vertices (as the line α_f). In general, however, that line can be dropped but one is then left with the overlap between the states on each side of the one-bar vertices. To clarify this point we show in fig. A4 the quantity

$$\sum_{\alpha_p} \sum_{\alpha_{c'} \ldots \alpha_{d'}} \langle \alpha_f | P^+(\alpha_a) P^+(\alpha_b) \ldots P^+(\alpha_{c'}) \ldots P^+(\alpha_{d'}) | 0 \rangle \langle \alpha_p | P^+(\alpha_{c'}) \ldots P^+(\alpha_{d'}) | 0 \rangle^*$$

$$\times \langle \alpha_p | P^+(\alpha_c) \ldots P^+(\alpha_d) | 0 \rangle$$

$$= \sum_{\alpha_{c'} \ldots \alpha_{d'}} \langle \alpha_f | P^+(\alpha_a) P^+(\alpha_b) \ldots P^+(\alpha_{c'}) \ldots P^+(\alpha_{d'}) | 0 \rangle D(\alpha_{c'} \ldots \alpha_{d'}; \alpha_c \ldots \alpha_d), \quad \text{(A.3)}$$

where the overlap

$$D(\alpha_{c'} \ldots \alpha_{d'}; \alpha_c \ldots \alpha_d) = \langle 0 | P(\alpha_{d'}) \ldots P(\alpha_{c'}) P^+(\alpha_c) \ldots P^+(\alpha_d) | 0 \rangle \quad \text{(A.4)}$$

is represented in fig. A4 by a square vertex. It is worthwhile to point out that if the states α_r in eq. (A.4) are such that $c' = c, \ldots, d' = d$, then the corresponding square vertex is symmetric with respect to the exchange of primed and unprimed states. Therefore, fig. 5 indicates that $D = D^+$, as indeed it is.

Although the general properties derived from figs. A3 and A4 are not very relevant to evaluate the dynamical matrix, they become important when deriving expressions for the metric matrix.

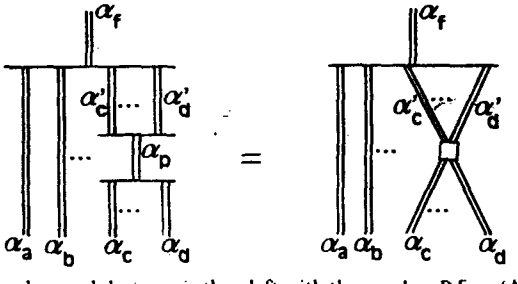

Fig. A4. The line α_p can be dropped, but one is then left with the overlap D [eq. (A.4)] represented by the square vertex.

References

1) A. de-Shalit, Phys. Rev. 122 (1961) 1530;
B. R. Mottelson, Proc. Int. Conf. on nuclear structure, Tokyo, 1967, ed. J. Sanada
2) S. K. M. Wong and A. P. Zuker, Phys. Lett. 36B (1971) 437
3) W. W. True and C. M. Ma, Phys. Rev. C9 (1974) 2275
4) C. M. Ko, T. T. S. Kuo and J. B. McGrory, Phys. Rev. C8 (1973) 2379
5) P. Ring and P. Schuck, Phys. Rev. C16 (1977) 801, and references therein
6) J. D. Vergados, Phys. Lett. 34B (1971) 458
7) A. Arima and F. Iachello, Phys. Rev. C16 (1977) 2085
8) P. F. Bortignon, R. A. Broglia, D. R. Bès and R. J. Liotta, Phys. Reports 30C (1977) 305
9) R. J. Liotta, C. Pomar and B. Silvestre-Brac, Symp. on pure and applied nuclear physics, Stockholm 1978; Nuov. Cim. Lett. 27 (1980) 100
10) R. J. Liotta and C. Pomar, Nucl. Phys. A362 (1981) 137
11) R. A. Broglia, K. Matsuyanagi, H. Sofia and A. Vitturi, Nucl. Phys. A348 (1980) 237
12) D. Strottman, Phys. Rev. 20C (1979) 1150
13) P. M. Morse and H. Feshbach, Methods of theoretical physics, vol. I (McGraw-Hill, NY, 1953)
14) C. Pomar and R. J. Liotta, Phys. Rev. C25 (1982) 1656
15) P. J. Brusaard and P. W. M. Glaudemans, Shell-model applications in nuclear spectroscopy (North-Holland, Amsterdam, 1977)
16) N. Auerbach and I. Talmi, Nucl. Phys. 64 (1965) 458
17) J. B. Ball, J. B. McGrory and J. S. Larsen, Phys. Lett. 41B (1972) 581
18) C. G. Lindén, I. Bergström, J. Blomqvist, K. G. Rensfelt and B. Fant, Z. Phys. A277 (1976) 273
19) G. G. Dussel and R. J. Liotta, Phys. Lett. 37B (1971) 477
20) R. J. Liotta and B. A. Silvestre-Brac, Nucl. Phys. A309 (1978) 301
21) P. F. Bortignon, R. A. Broglia, D. R. Bès, R. J. Liotta and V. Paar, Phys. Lett. 64B (1976) 24
22) D. R. Bès, R. A. Broglia, G. G. Dussel, R. J. Liotta and R. P. J. Perazzo, Nucl. Phys. A260 (1976) 77
23) D. J. Thouless, The quantum mechanics of many-body systems (Academic Press, New York, 1961)
24) B. D. Day, Rev. Mod. Phys. 39 (1967) 719
25) J. S. Briggs, Rev. Mod. Phys. 43 (1971) 189
26) D. M. Brink and G. R. Satchler, Angular momentum (Oxford UP, Oxford, 1968)
27) V. Paar, Nucl. Phys. A164 (1971) 576
28) P. Federman and S. Pittel, Phys. Rev. C20 (1979) 820
29) R. Vennink and P. W. M. Glaudemans, Z. Phys. A294 (1980) 241
30) F. Tondeaur, Nucl. Phys. A359 (1981) 278
31) J. P. Boisson, B. A. Silvestre-Brac and R. J. Liotta, Nucl. Phys. A330 (1979) 307
32) D. R. Bès, R. A. Broglia, O. Hansen and O. Nathan, Phys. Reports 34C (1977) 1
33) E. R. Flynn, R. A. Broglia, R. Liotta and B. S. Nilsson, Nucl. Phys. A343 (1980) 24
34) A. H. Wapstra and K. Bos, Atomic Data and Nucl. Data Tables 19 (1977) 185
35) A. Arima, H. Horiuchi, K. Kubodera and N. Takigawa, Adv. in Nucl. Phys. 5 (1972) 345
36) P. Kleinheinz, R. Broda, P. J. Daly, S. Lunardi, M. Ogawa and J. Blomqvist, Z. Phys. A286 (1978) 27
37) B. F. Bayman, A. S. Reiner and R. K. Sheline, Phys. Rev. 115 (1959) 1627
38) J. B. McGrory, Phys. Rev. Lett. 41 (1978) 533
39) S. A. Moszkowski, Phys. Rev. 19C (1979) 2387
40) G. Rosensteel and D. J. Rowe, Phys. Rev. Lett. 46 (1981) 1119
41) J. N. Ginocchio and I. Talmi, Nucl. Phys. A337 (1980) 431